Compatible Bridged Interphase with Enhanced Li Ion Migration for Durable Quasi-Solid-State Lithium Metal Batteries

Peng Chen[a], Hui Wang[a], Tianyu Wei[a], Shengliang Zhang[a], Bing Ding[a,b,c], Hui Dou[a,b,c*], and Xiaogang Zhang[a,b,c*]

[a]*Jiangsu Key Laboratory of Electrochemical Energy Storage Technologies, College of Materials Science and Technology, Nanjing University of Aeronautics and Astronautics, Nanjing 210016, P. R. China*

[b]*National Key Laboratory of Mechanics and Control for Aerospace Structures, Institute for Frontier Science, Nanjing University of Aeronautics and Astronautics, Nanjing 210016, P.R. China*

[c]*Shenzhen Research Institute, Nanjing University of Aeronautics and Astronautics, Shenzhen 518000, China*

*Corresponding author.
E-mail address: dh_msc@nuaa.edu.cn (Hui Dou); azhangxg@nuaa.edu.cn (Xiaogang Zhang)

1. Methods

1.1 Materials and battery assembly

LiFSI and PVDF-HFP (pellets), were purchased from Macklin. $Li_{6.75}La_3Zr_{1.75}Ta_{0.25}O_{12}$ (LLZTO), $LiFePO_4$ (LFP), $LiCoO_2$ (LCO) and 1M $LiPF_6$ in EC:EMC:DEC were purchased from Canrd. All were dried at 70 °C under vacuum for 24 h to remove moisture. N,N-dimethyl-Formamide (DMF, ≥99%) was bought from Macklin. Cu, Ni, Ag, Au, Pt foils (99.95%) were bought from ZhongNuo Advanced Material (Beijing) Technology Co.,Limited.

1.2 Preparation process of CPCEs

PVDF-HFP (1 g), LiFSI (0.5 g) and LLZTO (0.2 g) were added into 5 mL, 1 mL

and 1 mL of DMF, respectively, and stirred for 6 h to ensure uniform dispersion. The resulting mixture was then scraped onto a glass plate by using a 100 μm scraper. Then placed it in blast oven at 40 °C for 4 h, and the CPCEs was preliminary preparation. Subsequently, the CPCEs was vacuum dried at 80 °C for 48 h to remove residual DMF.

1.3 Preparation process of M@CPCEs

The targets (Cu, Ni, Ag, Au, Pt foils, respectively) were assembled. Next, the obtained CPCEs was fixed on a sample stage and together in the magnetron sputtering instrument chamber. The process parameters for magnetron sputtering were set: argon atmosphere pressure of 0.1 Pa, electrical current of 40 mA, sputtering time of 30 s.

1.4 Preparation of LFP or LCO cathode

90 wt% LFP or LCO, 5 wt% Super P, 5 wt% PVDF/NMP (30 mg mL^{-1}) were mixed for 24 h. The resulting mixture was then scraped onto carbon coated aluminum foil. Subsequently, the cathode was air drying for 6 h and then vacuum dried at 110 °C for 12 h to remove residual NMP. The mass loading of LFP cathode is over 12.5 mg cm^{-2}. While the ~ 2.0 mg cm^{-2} for cyclic voltammetry (CV) test.

1.5 Battery assembly

Placing the Li metal on the M@CPCEs. And then, cut them into composite Li/M@CPCEs.

The assembly of the Li|M@CPCEs|Li symmetrical cell consists of two pieces of Li/M@CPCEs, with 10 μL of electrolyte addition.

The assembly of the Li|M@CPCEs|LFP quasi-solid-state lithium metal batteries consists of a single Li/M@CPCEs , with the CPCEs side facing the LFP cathode. 2.0 μL mg^{-1} of electrolyte was then added to the cell.

The assembly of the Li|M@CPCEs|LCO liquid-state Li metal batteries consists

of a single Li/M@CPCEs and PP separator. 40 μL of electrolyte was then added to the cell.

2. Electrochemical measurements

The in situ DRT were calculated from the electrochemical impedance spectroscopy data obtained by an electrochemical station (VMP3, BioLogic Science Instruments) from 7 MHz to 100 mHz at 25 °C. The linear sweep voltammetry curves were measured at a scan rate of 0.1 mV s^{-1}~1.0 mV s^{-1} by using VMP3 at 25 °C. The cyclic voltammogram curves of the Li||LFP quasi-solid-state batteries between the potential ranges 2.5-4.0 V (V vs. Li/Li^+). The galvanostatic charge/discharge performance of the Li|M@CPCEs|LFP cell between the potential ranges 2.5-4.0 V (V vs. Li/Li^+) at 30 °C was examined by battery tester (LAND CT2001A).

The Li||Li symmetric cell were prepared and polarized at a certain voltage (ΔV = 10 mV) for 3600 s to test the t_{Li+}. Formula are as follows:

$$t_+ = \frac{I_s(\Delta V - I_0 R_{el}^0)}{I_0(\Delta V - I_s R_{el}^s)}$$

R_0 and R_s are the initial and steady-state interface impedances, I_0 and I_s are the initial and steady-state currents in the chronoamperometry method, and ΔV is the potential difference in the chronoamperometry method.

3. Calculation method

Our spin-polarized density functional theory (DFT) calculations were carried out in the Vienna ab initio simulation package (VASP) based on the plane-wave basis sets with the projector augmented-wave metho. The exchange-correlation potential was treated by using a generalized gradient approximation (GGA) with the Perdew-Burke-Ernzerhof (PBE) parametrization. Meanwhile, a vacuum region of about 15 Å was

applied to avoid the interaction between adjacent images. The energy cutoff was set to be 450 eV. The Brillouin-zone integration was sampled with a Γ-centered Monkhorst-Pack mesh of 1 × 1 × 1. The structures were fully relaxed until the maximum force on each atom was less than 0.03 eV $Å^{-1}$, and the energy convergent standard was 10^{-5} eV.

The adsorption energy Eads can be defined as, Eads = E*M - E* - EM, where E*M stands for the energy of the monolayer with the adsorbed M molecule, E* is the energy of surface, and EM is the energy of a M molecule under vacuum.

AIMD simulations used a C-point Brillouin zone for all interfacial supercell models. The DFT-D3 method was used to correct vander Waals forces. VESTA enables the visualization of all structures in a VASP calculation.

4. Materials characterization

Fourier transform-infrared spectrum was tested on X-ray photoelectron spectroscopy (XPS) was carried out with a Perkin-Elmer PHI 550 with Al-Kα as the X-ray source. Scanning electron microscopy (SEM) and the Time of Flight Secondary Ion Mass Spectrometry (TOF-SIMS) was characterized on the TESCAN LYRA3 GMU. 3D confocal laser microscopy (CLSM) was characterized on the Keyence VK-X1000. Atomic Force Microscope (AFM) was characterized on the SPM9700-HT.

Supplementary Figure

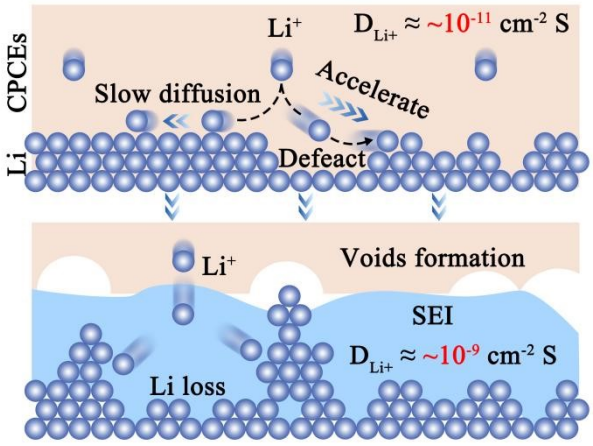

Fig. S1. Schematic diagram illustrating the interface ion transport rate of CPCEs-based QSSLMBs before and after cycling.

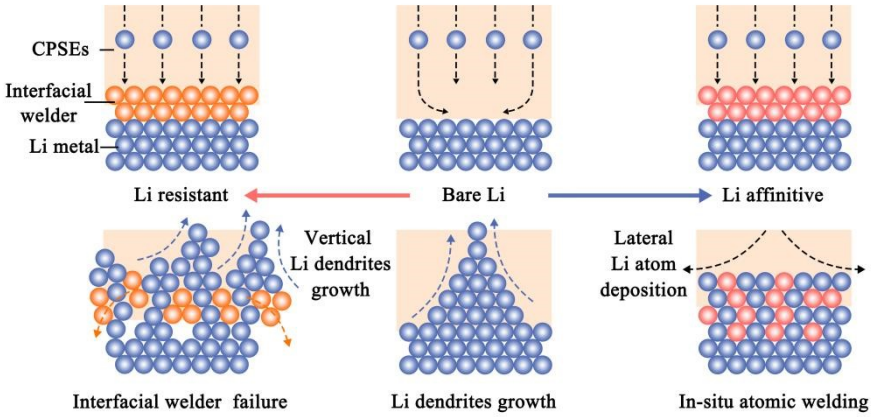

Fig. S2. Schematic diagram illustrating the working mechanism of nano metal layer with Li resistant/affinitive in the CPCEs-based QSSLMBs.

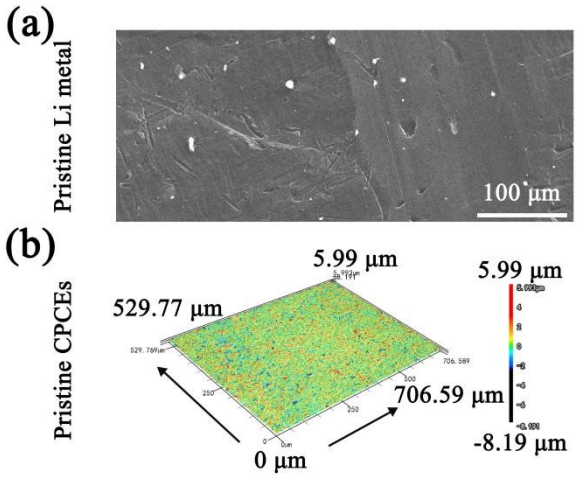

Fig. S3. (a) SEM image of bare Li metal. (b) 3D confocal laser microscopy (CLSM) image of CPCEs.

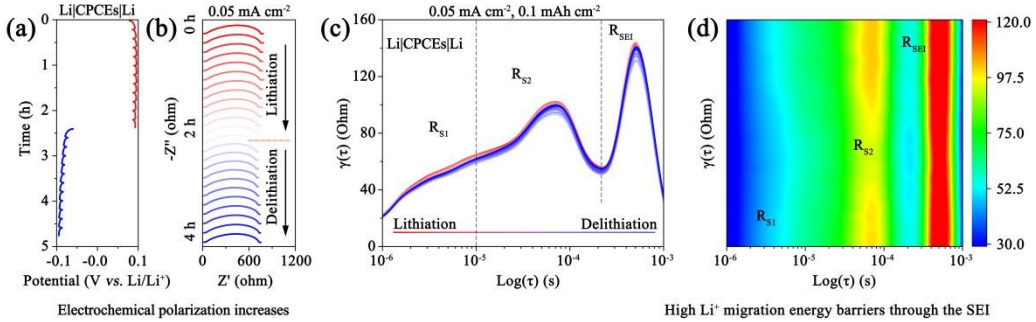

Fig. S4. (a) Voltage profiles, (b) EIS and (c) DRT and (d) their contour map of Li|CPCEs|Li symmetric cell under a cyclic current of 0.05 mA cm^{-2}, 0.1 mAh cm^{-2}, at 25°C.

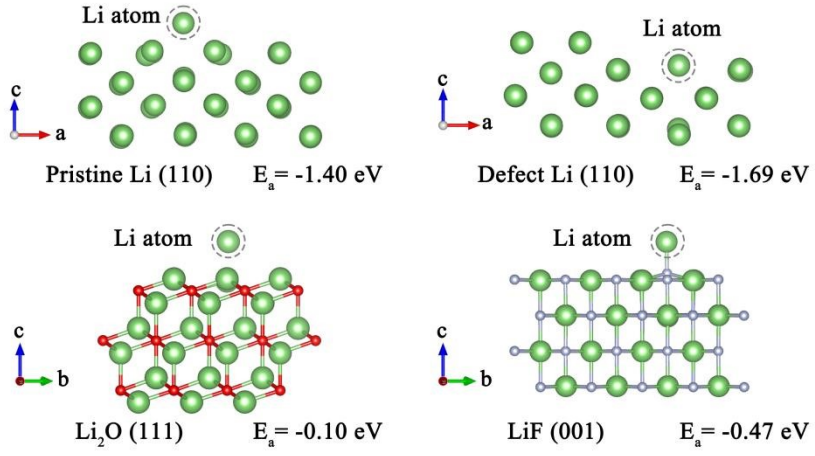

Fig. S5. Adsorption energy for Li^0 on the pristine Li, defect Li, Li_2O, and LiF

substrates.

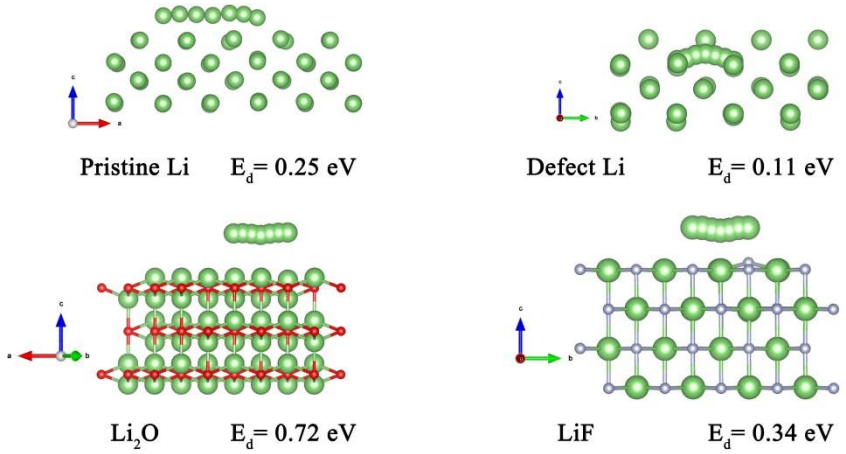

Fig. S6. Diffusion energy for Li^0 on the surface of pristine Li, defect Li, Li_2O, and LiF substrates.

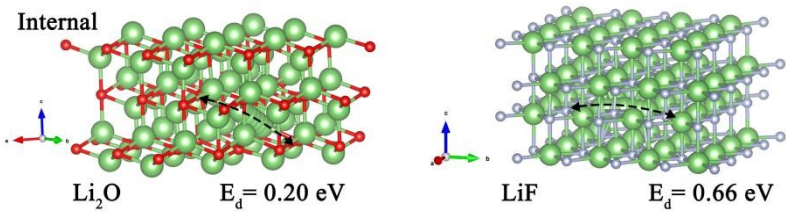

Fig. S7. Diffusion energy for Li^0 in the Li_2O, and LiF substrates.

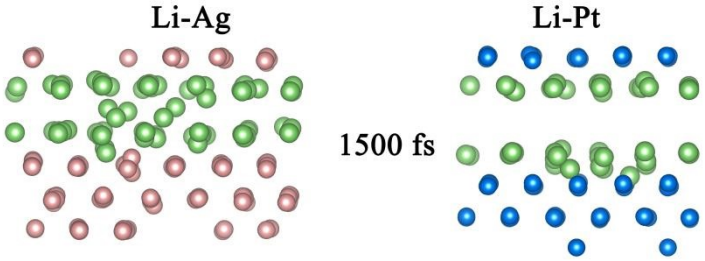

Fig. S8. AIMD simulation of Li-Ag, Li-Pt alloy in 1500 fs.

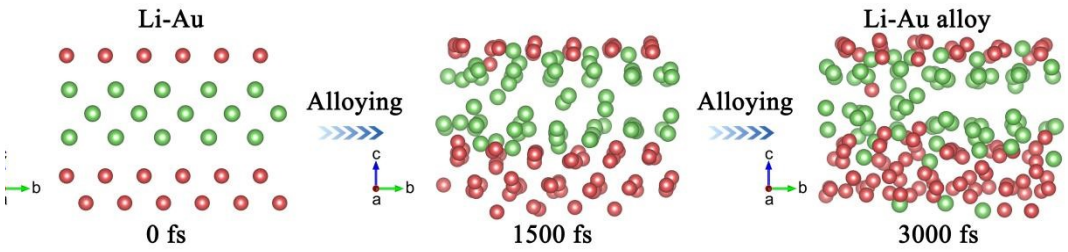

Fig. S9. AIMD simulation of Li-Au alloying process.

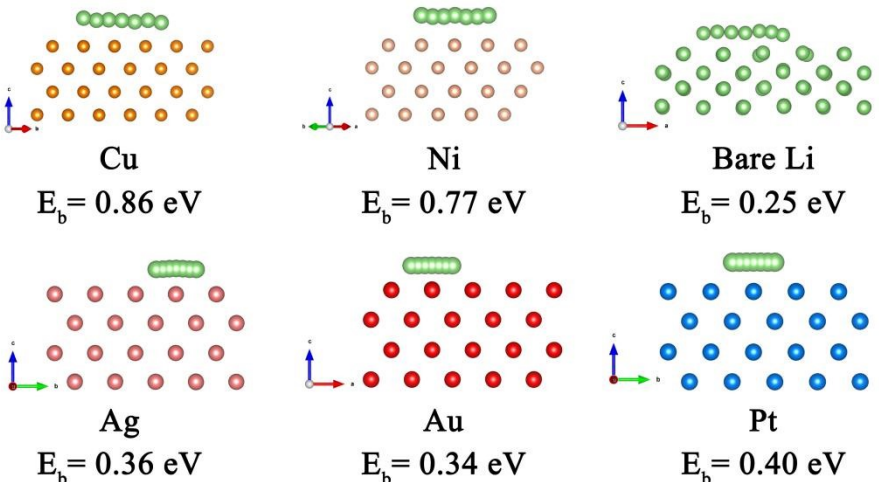

Fig. S10. Diffusion energy for Li^0 on the surface of metal substrates.

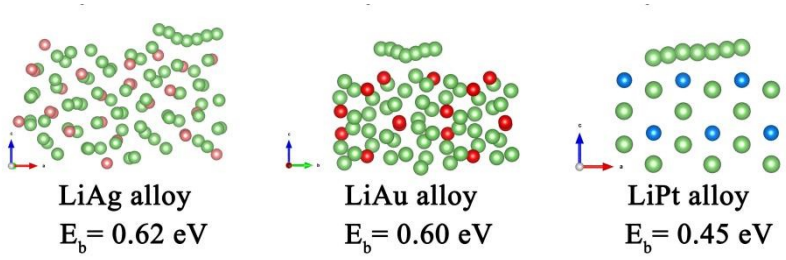

Fig. S11. Diffusion energy for Li^0 on the surface of Li-M alloy substrates.

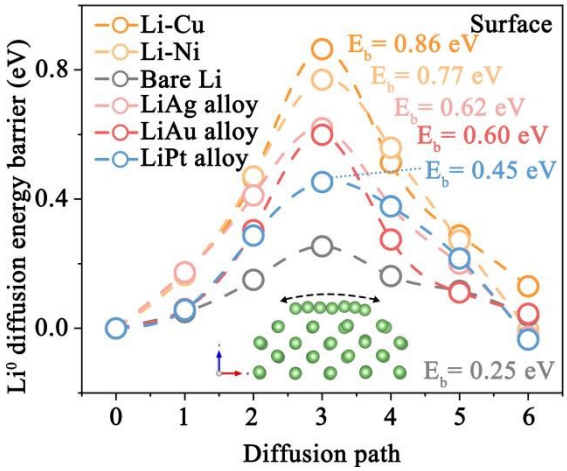

Fig. S12. Diffusion energy for Li^0 on the surface of different substrates.

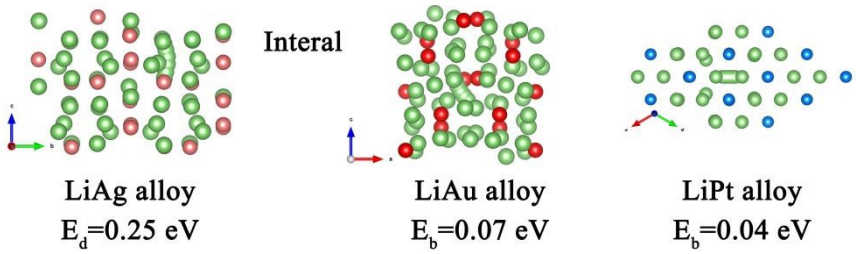

Fig. S13. Diffusion energy for Li^0 in the Li-M alloy substrates.

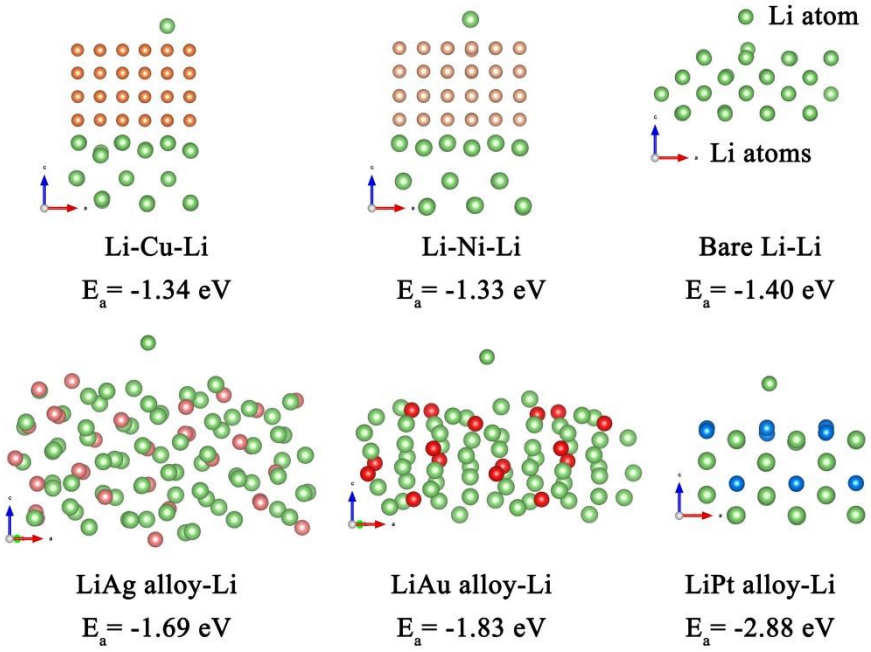

Fig. S14. Adsorption energy for Li^0 on the surface of different substrates.

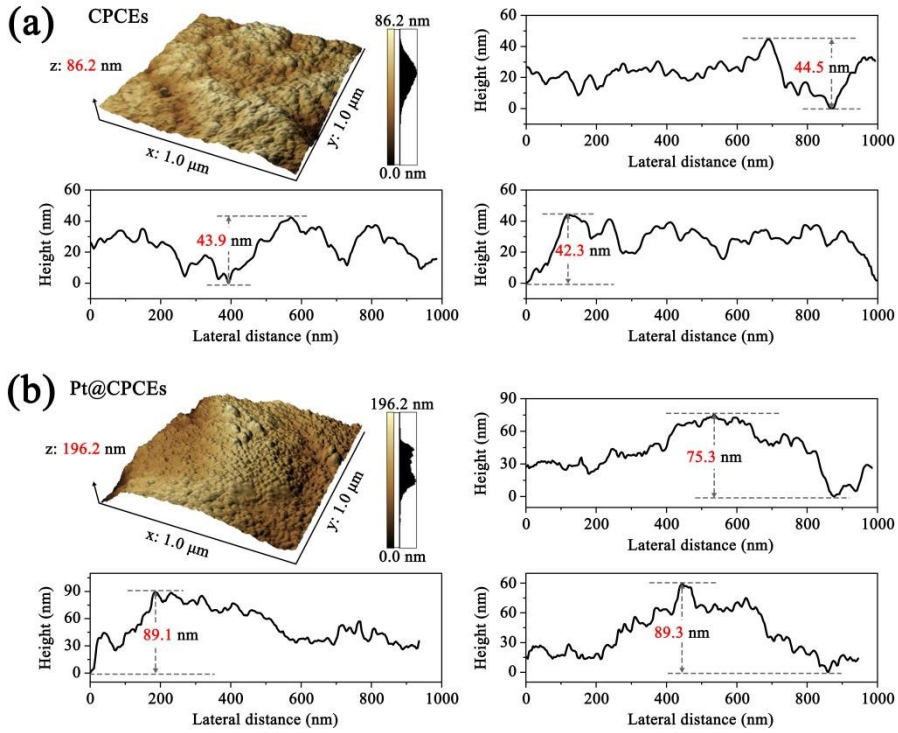

Fig. S15. Atomic Force Microscope (AFM) image of CPCEs and Pt@CPCEs.

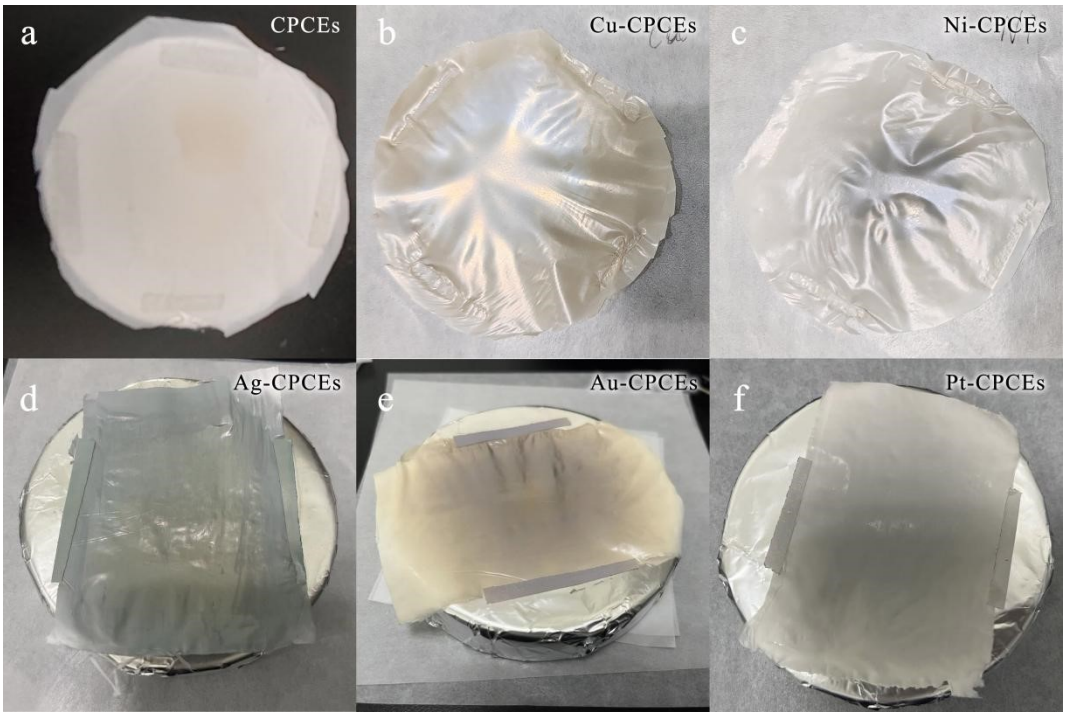

Fig. S16. Digital pictures of M@CPCEs.

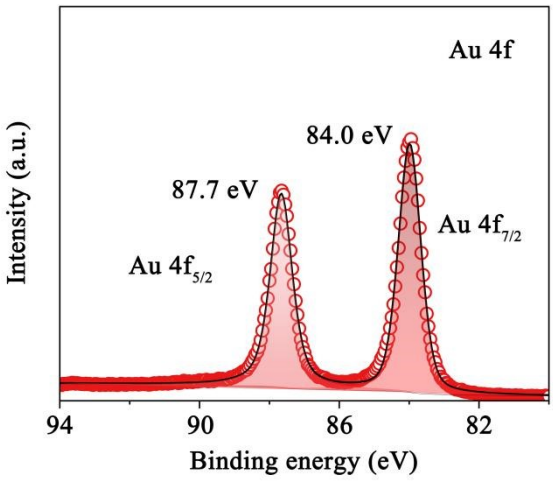

Fig. S17. XPS profiles of Au 4f of Au@CPCEs.

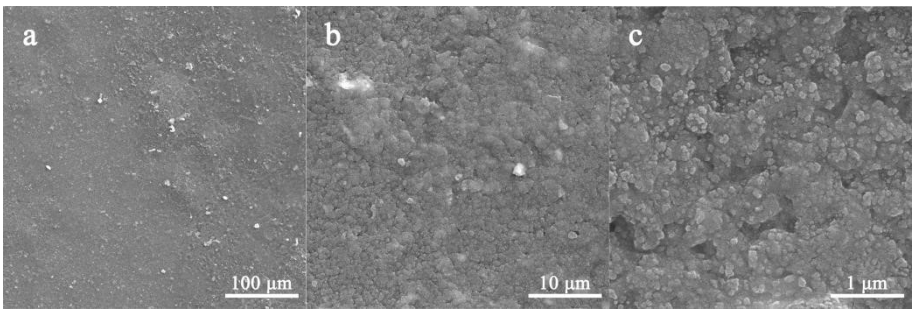

Fig. S18. SEM images and corresponding element mapping of bare CPCEs.

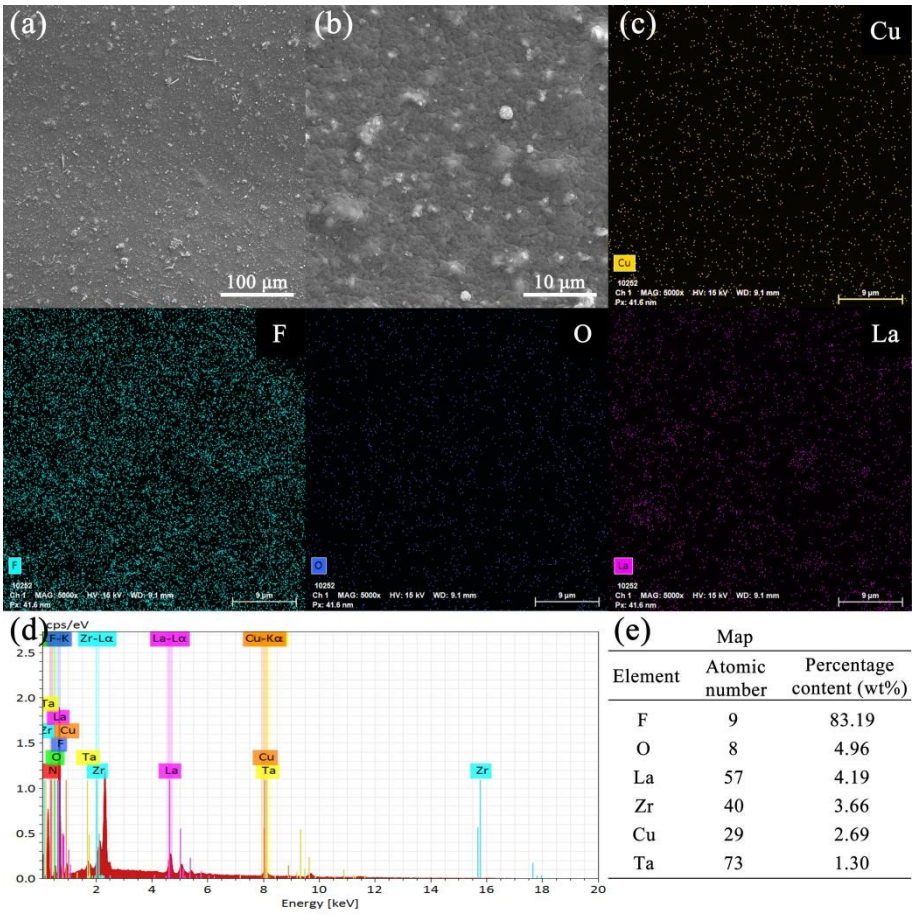

(e) Map

Element	Atomic number	Percentage content (wt%)
F	9	83.19
O	8	4.96
La	57	4.19
Zr	40	3.66
Cu	29	2.69
Ta	73	1.30

Fig. S19. SEM images and corresponding element mapping of Cu@CPCEs.

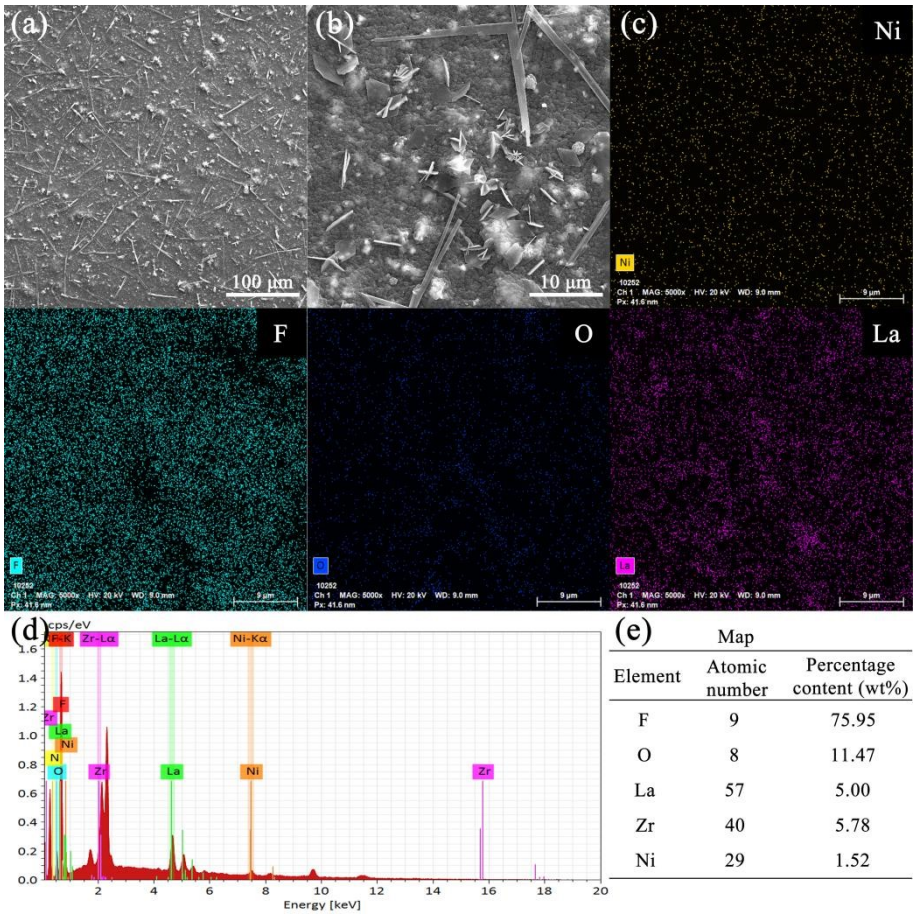

(e) Map

Element	Atomic number	Percentage content (wt%)
F	9	75.95
O	8	11.47
La	57	5.00
Zr	40	5.78
Ni	29	1.52

Fig. S20. SEM images and corresponding element mapping of Ni@CPCEs.

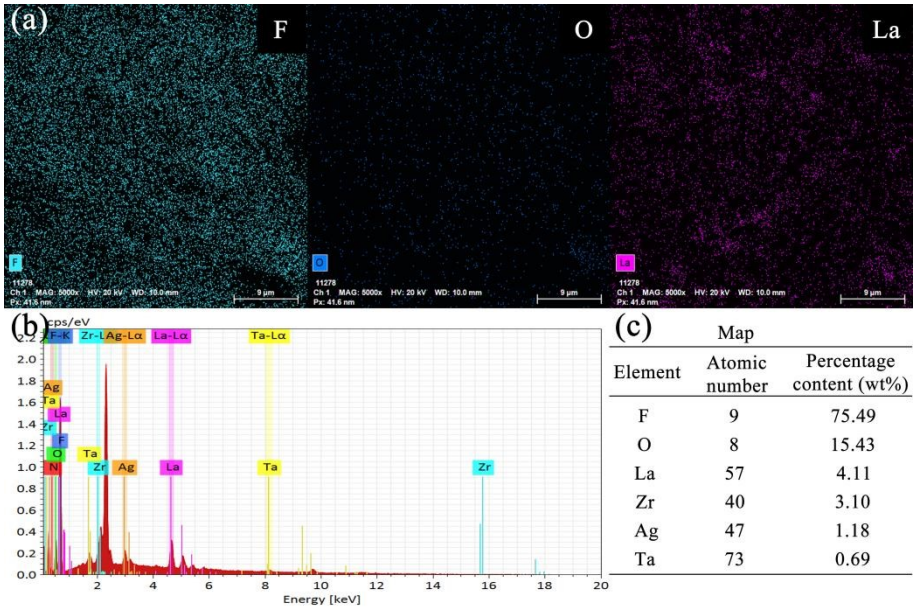

(c) Map

Element	Atomic number	Percentage content (wt%)
F	9	75.49
O	8	15.43
La	57	4.11
Zr	40	3.10
Ag	47	1.18
Ta	73	0.69

Fig. S21. SEM images and corresponding element mapping of Ag@CPCEs.

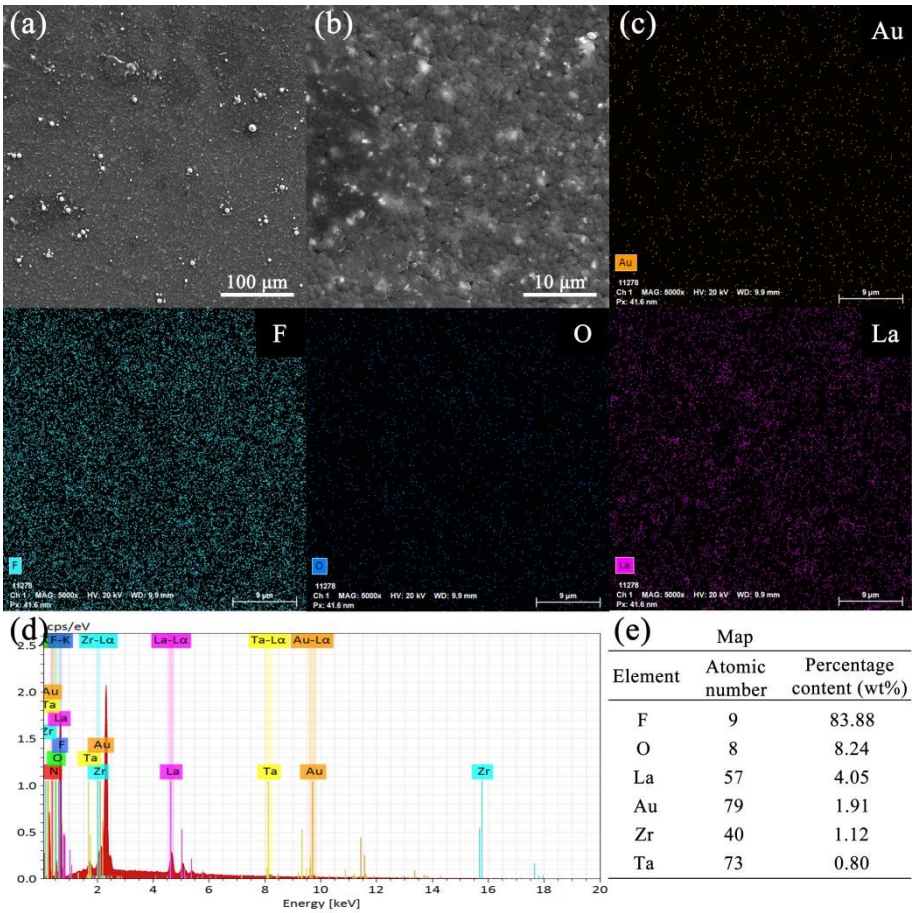

(e) Map

Element	Atomic number	Percentage content (wt%)
F	9	83.88
O	8	8.24
La	57	4.05
Au	79	1.91
Zr	40	1.12
Ta	73	0.80

Fig. S22. SEM images and corresponding element mapping of Au@CPCEs.

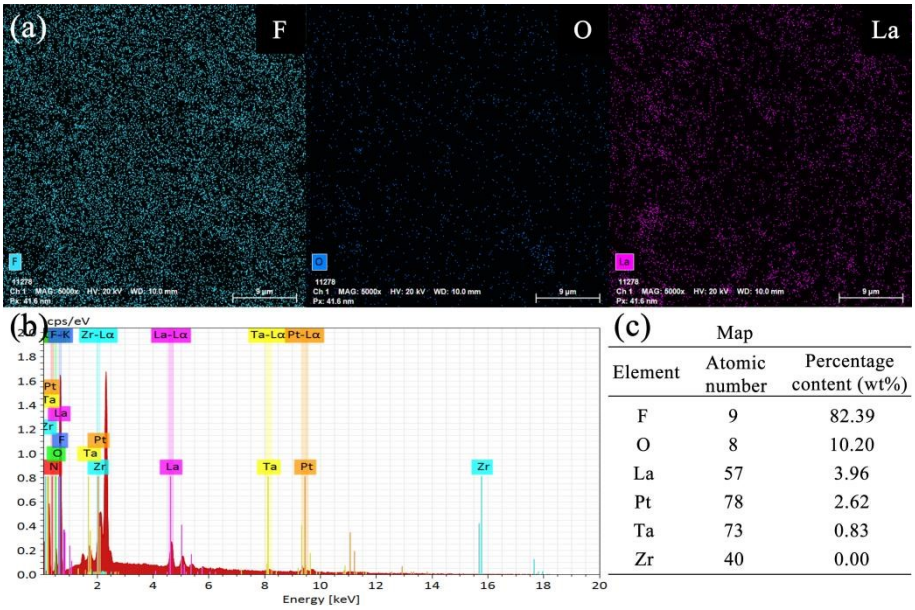

(c) Map

Element	Atomic number	Percentage content (wt%)
F	9	82.39
O	8	10.20
La	57	3.96
Pt	78	2.62
Ta	73	0.83
Zr	40	0.00

Fig. S23. SEM images and corresponding element mapping of Pt@CPCEs.

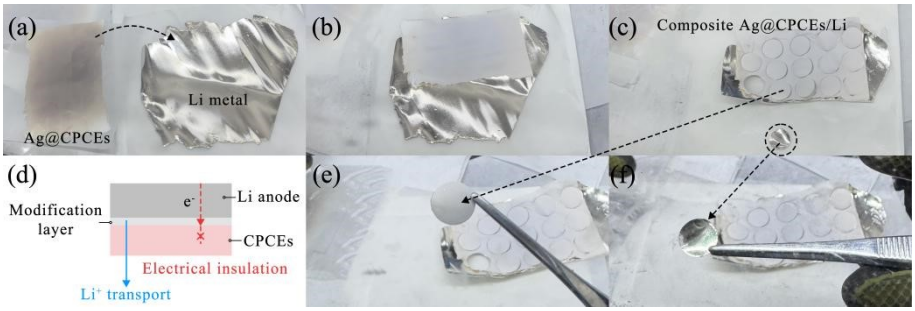

Fig. S24. Schematic illustration of M@CPCEs-based Li||Li symmetric cell fabrication.

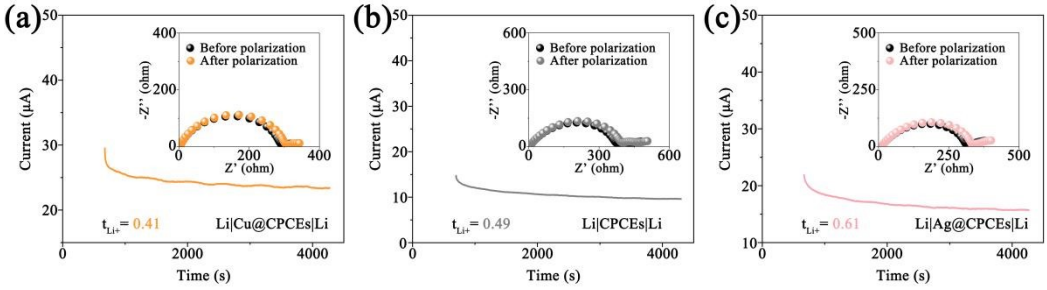

Fig. S25. Chronoamperometry curve and AC impedance spectra before and after polarization of the (a) Cu@CPCEs, (b) CPCEs, (c) Ag@CPCEs based Li||Li symmetric cells.

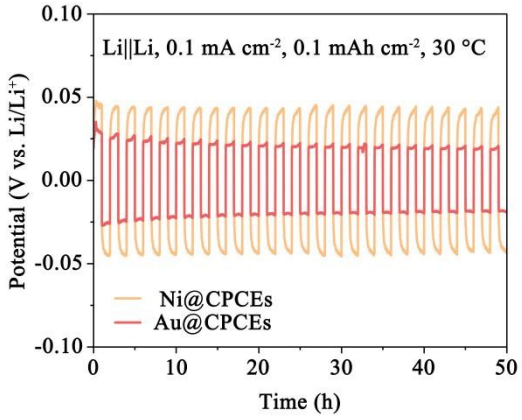

Fig. S26. Voltage profiles of Li|M@CPCEs|Li symmetric cells under 0.1 mA cm^{-2}, 0.1 mAh cm^{-2}, at 30 °C.

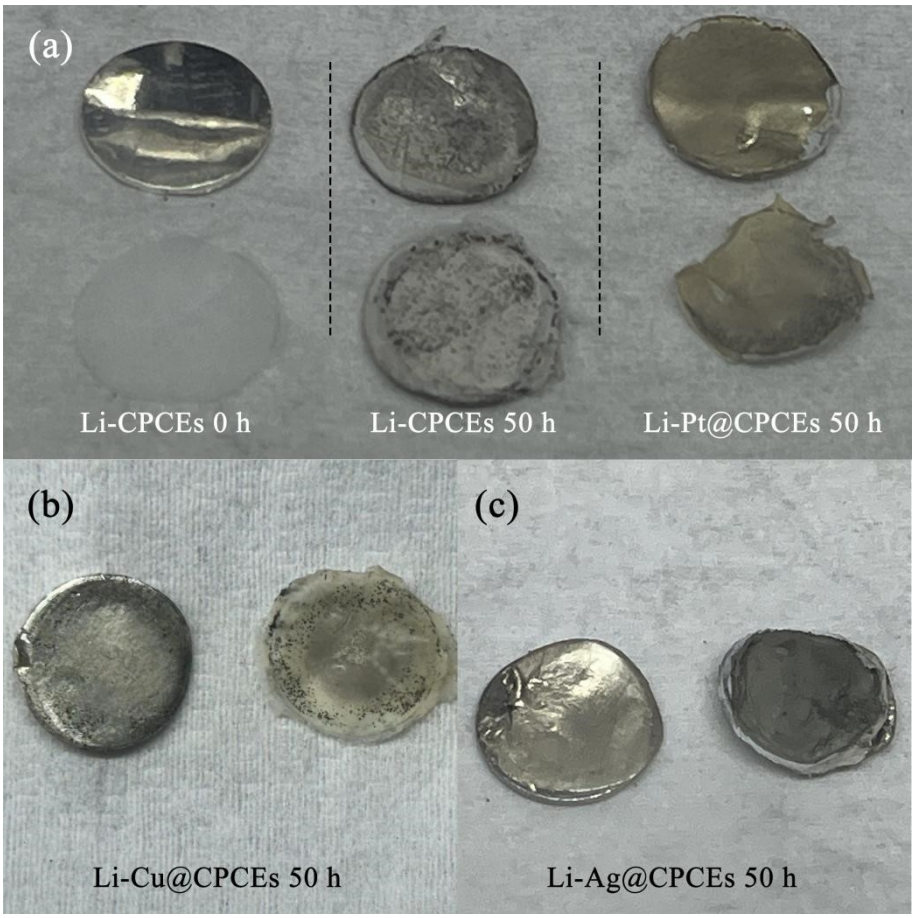

Fig. S27. Digital pictures of Li and M@CPCEs after cycling.

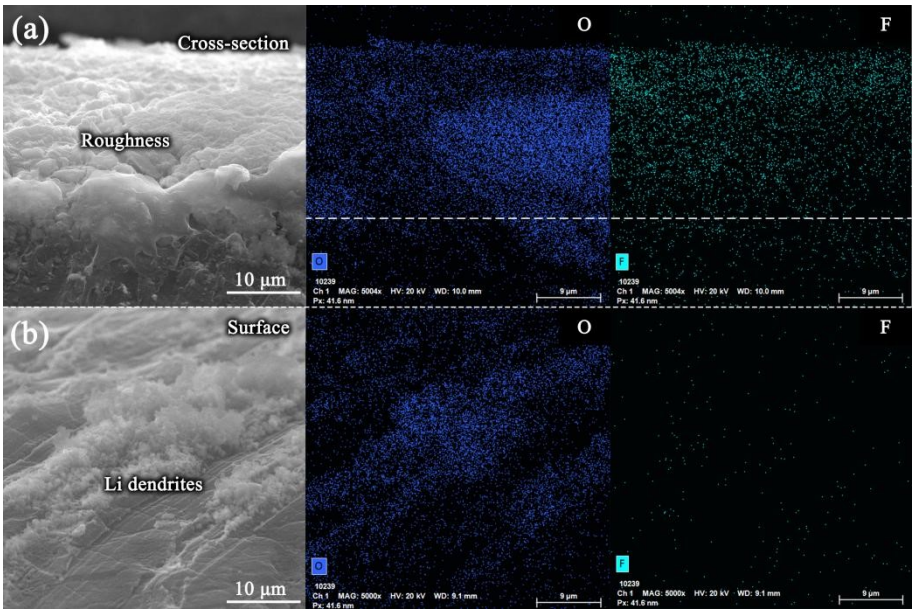

Fig. S28. SEM images and corresponding element mapping of Li metal in Li|CPCEs|Li symmetric cell after cycling.

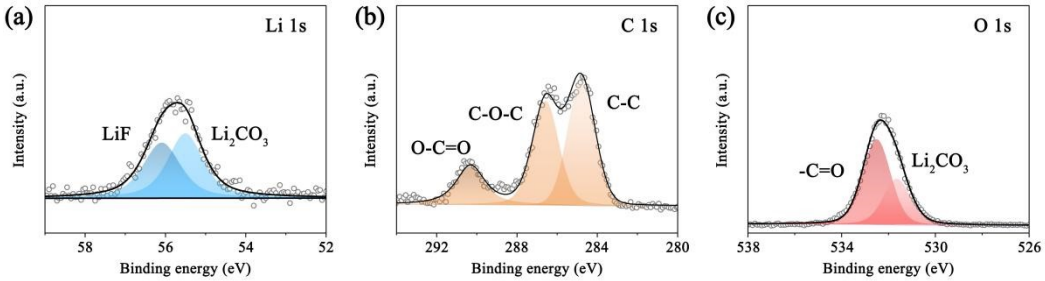

Fig. S29. XPS profiles of (a) Li 1s, (b) C 1s, and (c) O 1s on the Li metal in Li|CPCEs|Li after cycling.

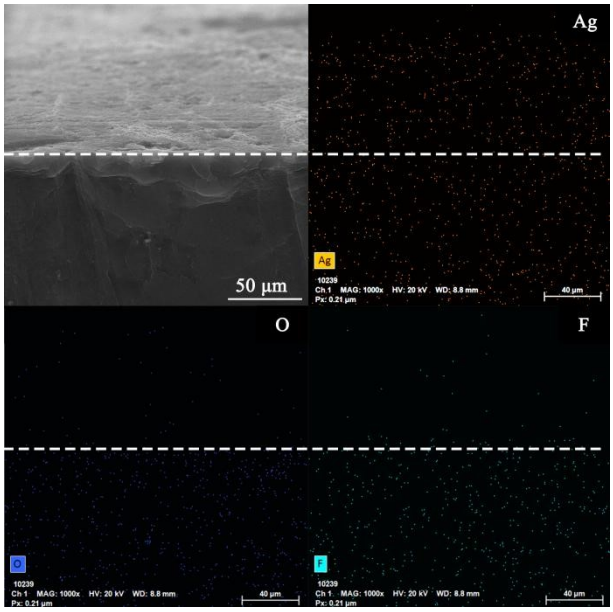

Fig. S30. SEM images and corresponding element mapping of Li metal in Li|Ag@CPCEs|Li symmetric cell after cycling.

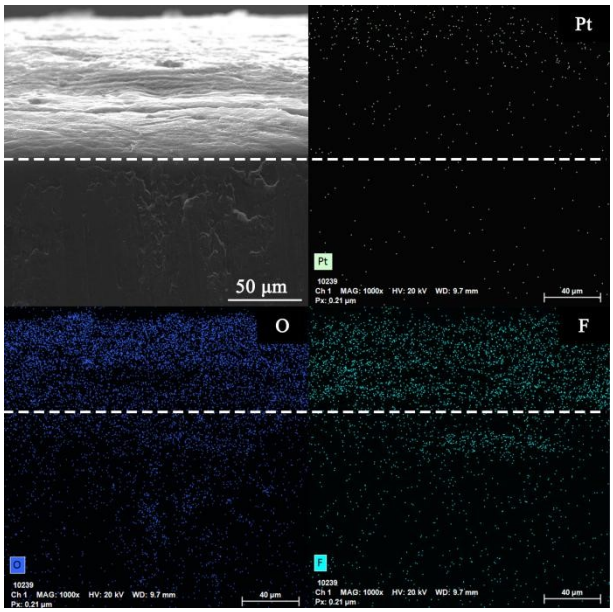

Fig. S31. SEM images and corresponding element mapping of Li metal in Li|Pt@CPCEs|Li symmetric cell after cycling.

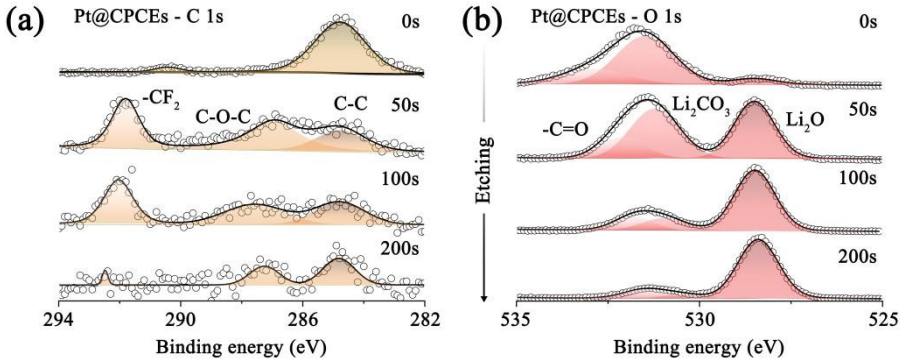

Fig. S32. XPS profiles of (a) C 1s and (b) O 1s on the Li metal with etching after cycling.

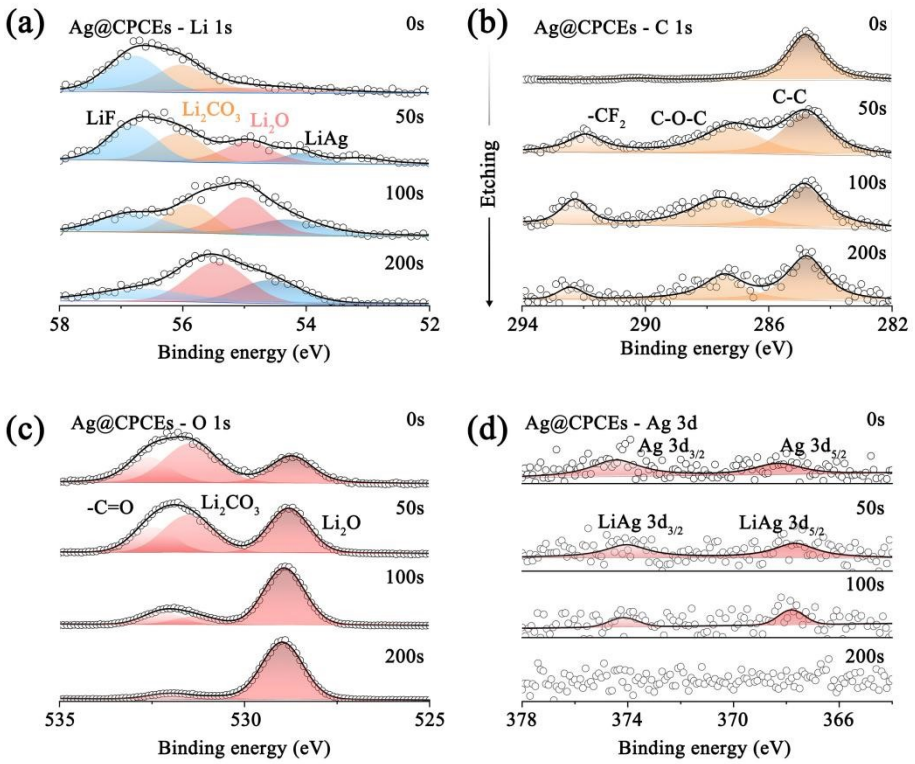

Fig. S33. XPS profiles of (a) Li 1s, (b) C 1s, (c) O 1s, and (d) Ag 3d on the Li metal with etching after cycling.

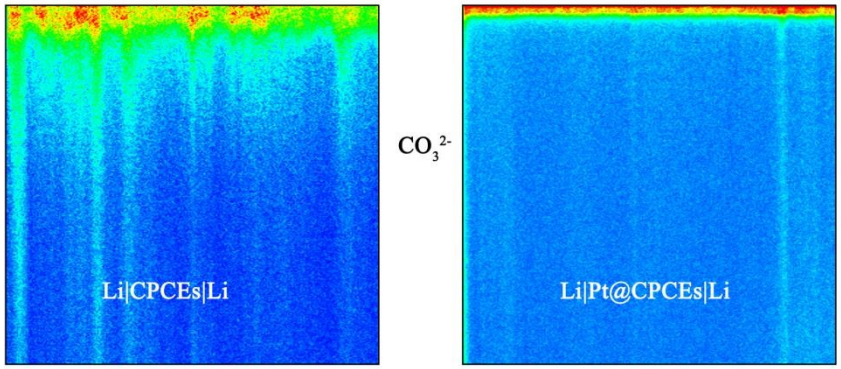

Fig. S34. The TOF-SIMS sputtered volumes of Li metal without/with Pt@CPCEs.

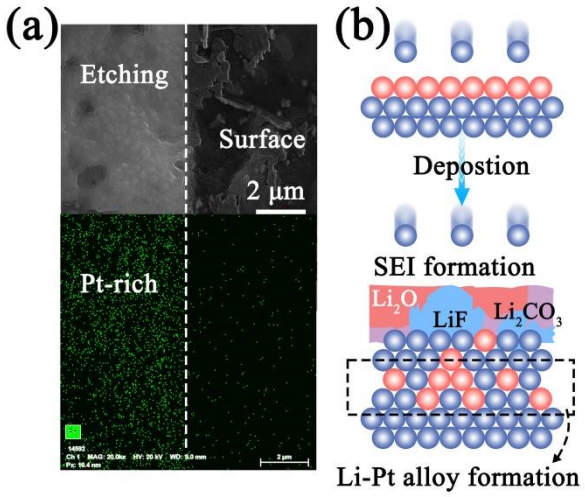

Fig. S35. (a) SEM images and corresponding element mapping of Li metal in Li|Pt@CPCEs|Li symmetric cell after cycling with etching. (b) Schematic diagram of the structure and formation of the interfacial ion migration modulator.

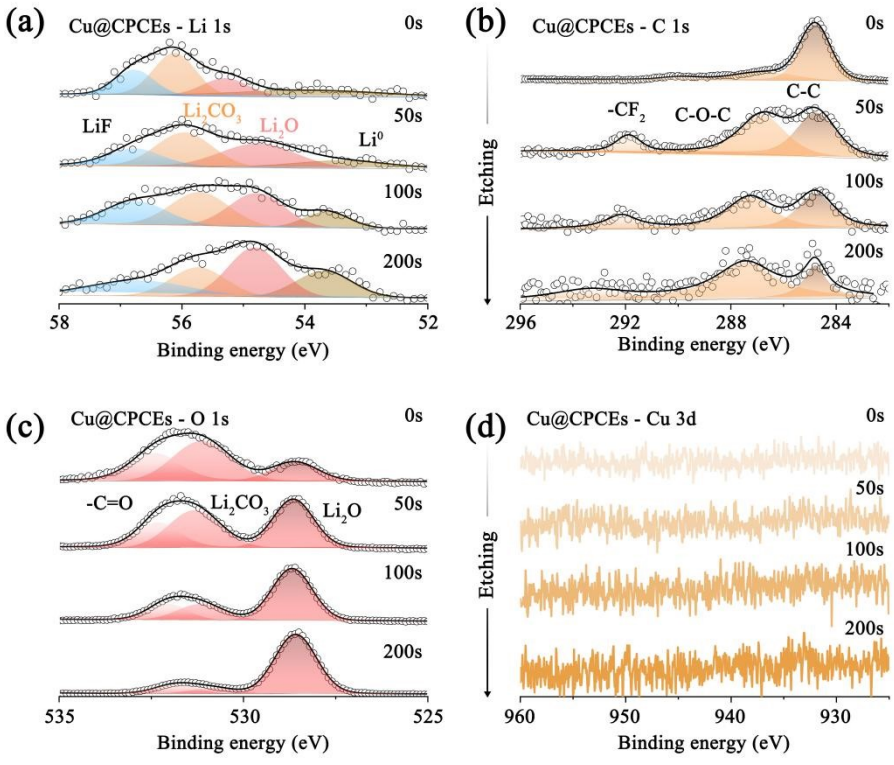

Fig. S36. XPS profiles of (a) Li 1s, (b) C 1s, (c) O 1s, and (d) Cu 3d on the Li metal with etching after cycling.

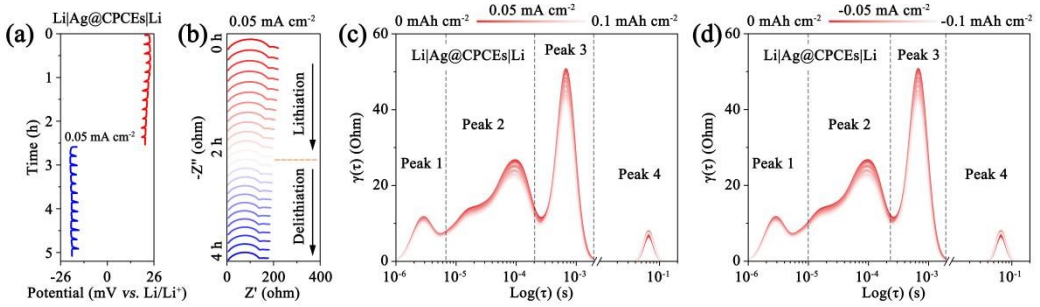

Fig. S37. (a) Voltage profiles, (b) EIS and (c-d) DRT of Li|Ag@CPCEs|Li symmetric cell under 0.05 mA cm^{-2}, 0.1 mAh cm^{-2}, at 25°C.

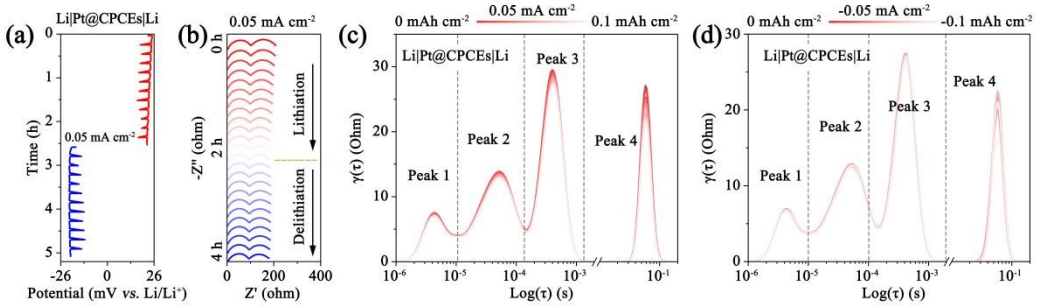

Fig. S38. (a) Voltage profiles, (b) EIS and (c-d) DRT of Li|Pt@CPCEs|Li symmetric cell under 0.05 mA cm^{-2}, 0.1 mAh cm^{-2}, at 25°C.

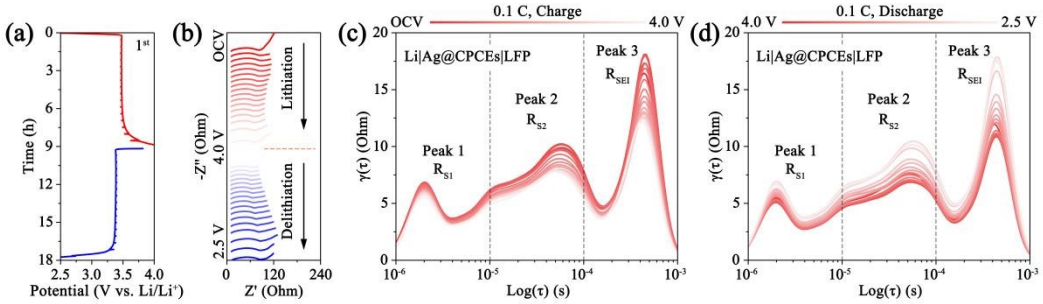

Fig. S39. (a) Voltage profiles, (b) EIS and (c-d) DRT of Li|Ag@CPCEs|LFP at 0.1 C.

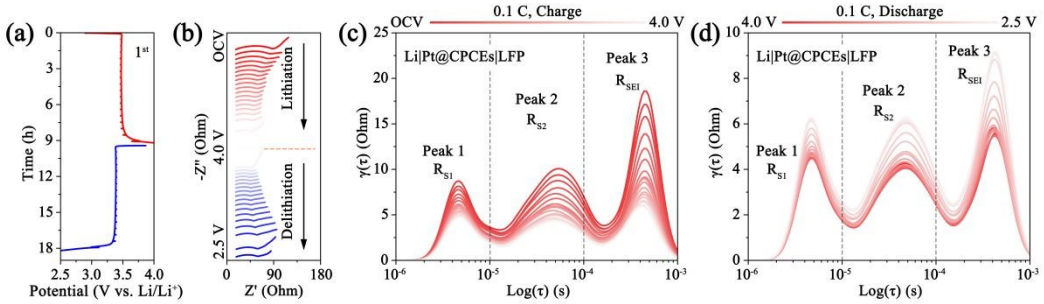

Fig. S40. (a) Voltage profiles, (b) EIS and (c-d) DRT of Li|Pt@CPCEs|LFP at 0.1 C.

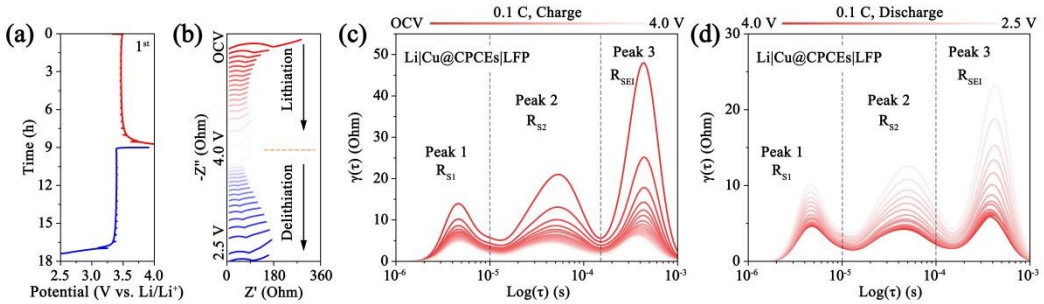

Fig. S41. (a) Voltage profiles, (b) EIS and (c-d) DRT of Li|Cu@CPCEs|LFP at 0.1 C.

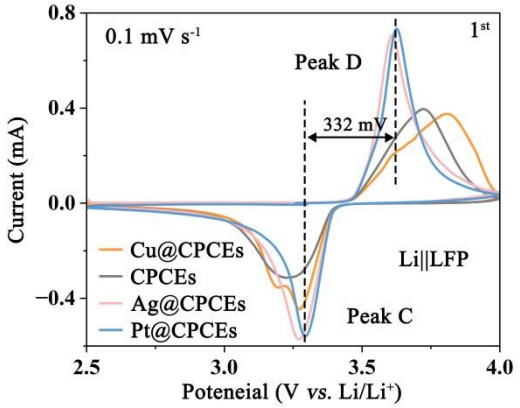

Fig. S42. CV measurements of Li|M@CPCEs|LFP at the sweep rate of 0.1 mV s^{-1}.

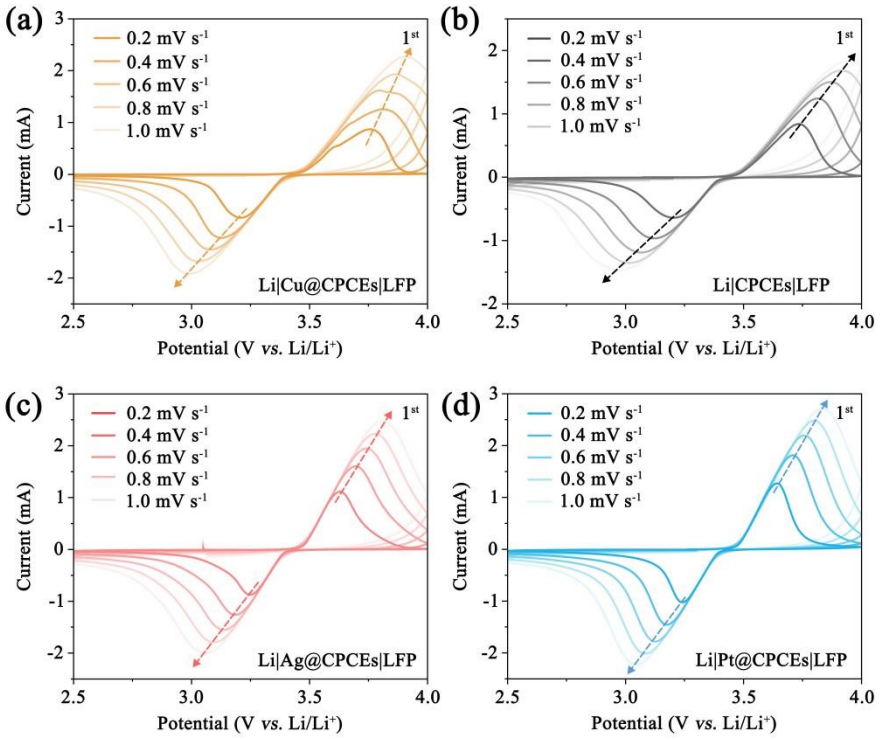

Fig. S43. CV measurements of Li|M@CPCEs|LFP at the sweep rate of 0.2-1.0 mV s^{-1}.

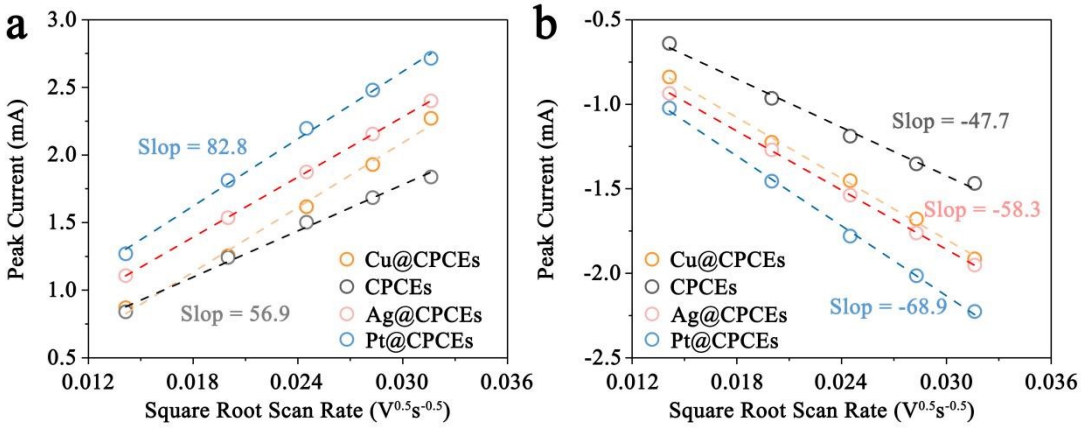

Fig. S44. Ip slope chart of Li|M@CPCEs|LFP.

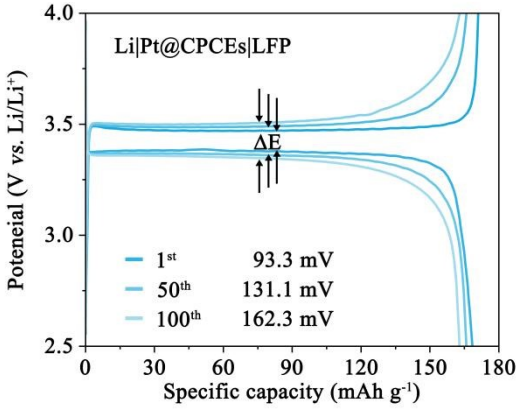

Fig. S45. Galvanostatic charge/discharge curves of Li|Pt@CPCEs|LFP at 0.2 C.

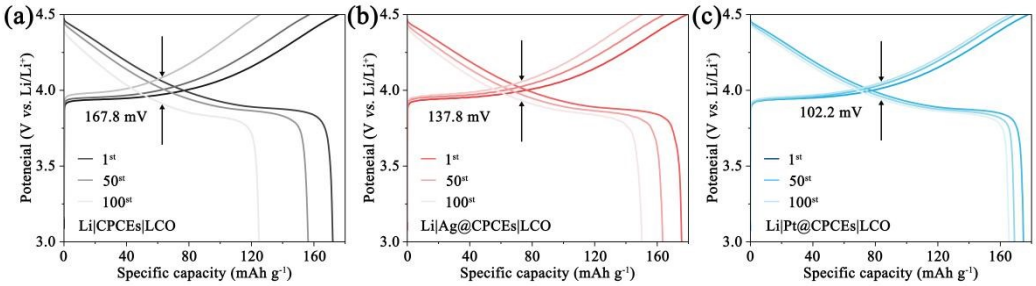

Fig. S46. Galvanostatic charge/discharge curves of Li|M@CPCEs|LCO at 0.2 C.

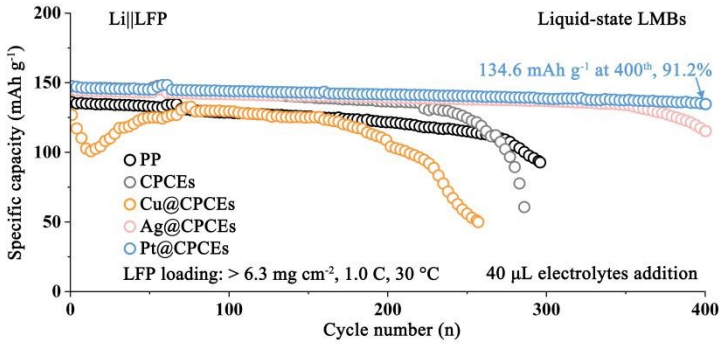

Fig. S47. Long-cycle tests of the Li||LFP liquid-state LMBs with interfacial ion migration modulator at 30 °C.